Supplementary Information

Extremely Low-power-consumption Reconfigurable Two-dimensional Tellurene Artificial Synapse for Bio-inspired Wearable Edge Computing

Bolim You[†⊥], Jeechan Yoon[†⊥], Yuna Kim[†], Mino Yang[§], Jina Bak[†], Jihyang Park[†], Unjeong Kim[¶*], Myung Gwan Hahm[†‖*], Moonsang Lee[†*]

[†]Department of Materials Science and Engineering, Inha University, 100 Inha-ro, Michuhol-gu, Incheon 22212, Republic of Korea

[§]Korea Basic Science Institute Seoul, 6-7, Goryeodae-ro 22-gil, Seongbuk-gu, Seoul 02841, Republic of Korea

[‖]Institute for Bio-Medical and Translational Health Care, Inha University Hospital, 27 Inhang-ro, Jung-gu, Incheon, Republic of Korea 22332

[¶]Department of physics, Dongguk university, Seoul 04620, republic of korea

* Corresponding authors.

E-mail addresses: ujjane.kim@dongguk.edu (U. Kim), mghahm@inha.ac.kr (M.G. Hahm), mslee@inha.ac.kr (M. Lee)

[⊥]Bolim You and Jeechan Yoon contributed equally to this paper.

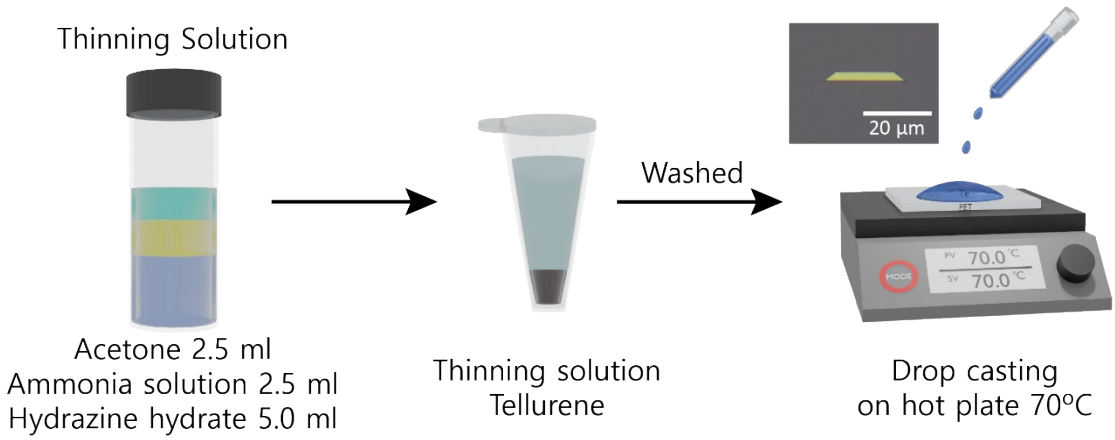

Figure S1. (a) Schematic of solvent-assisted thinning process and drop casting.

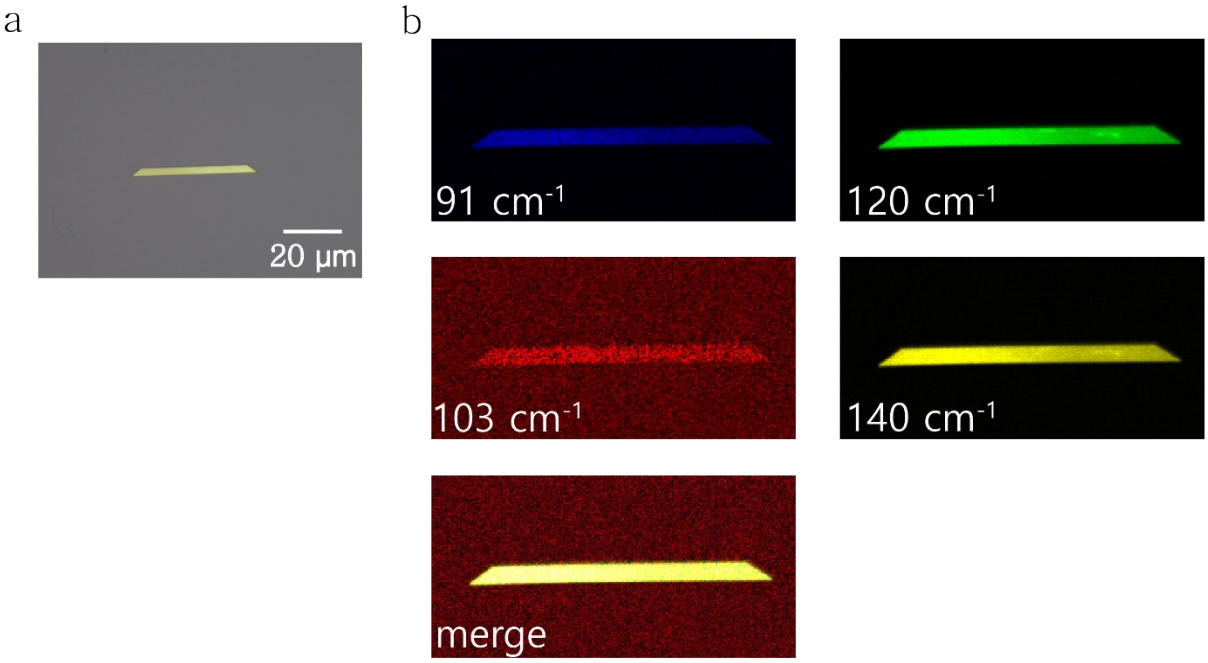

Figure S2. (a) Optical image of 2D tellurene (Te) on Si/SiO_2(100 nm). (b) Raman mapping images of 2D Te.

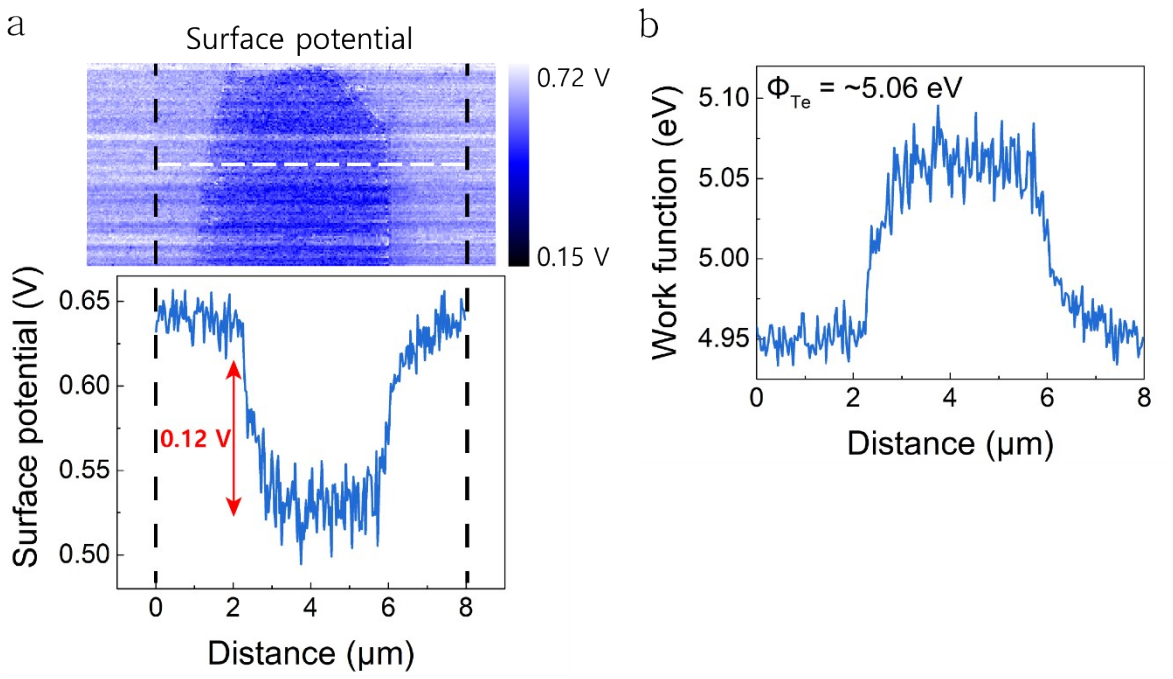

Figure S3. (a) Surface potential and (b) work function of 2D Te on p-Si measured through Kelvin probe force microscopy (KPFM). The Te work function is ~5.06 eV.

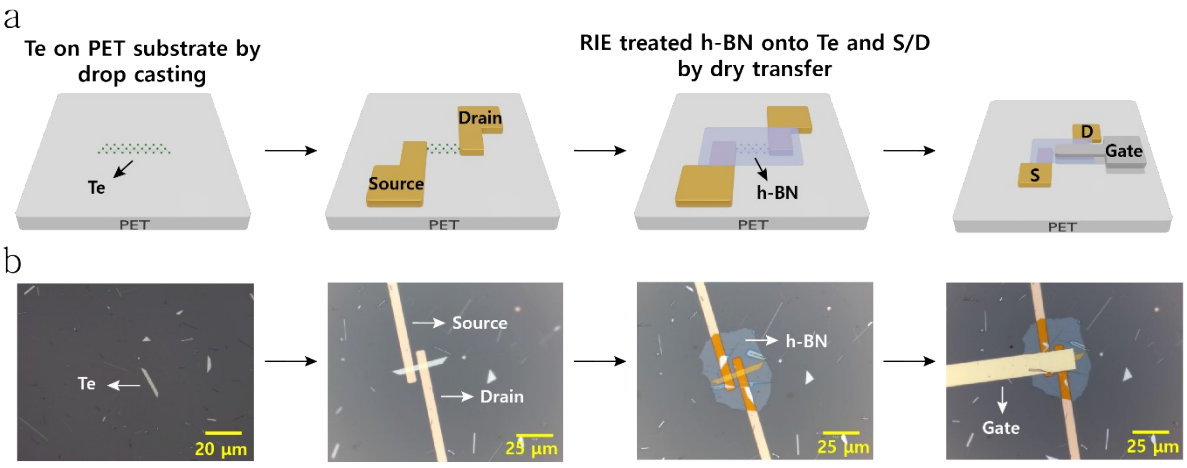

Figure S4. (a) Schematics and (b) optical images of the fabrication method for the flexible 2D Te transistor.

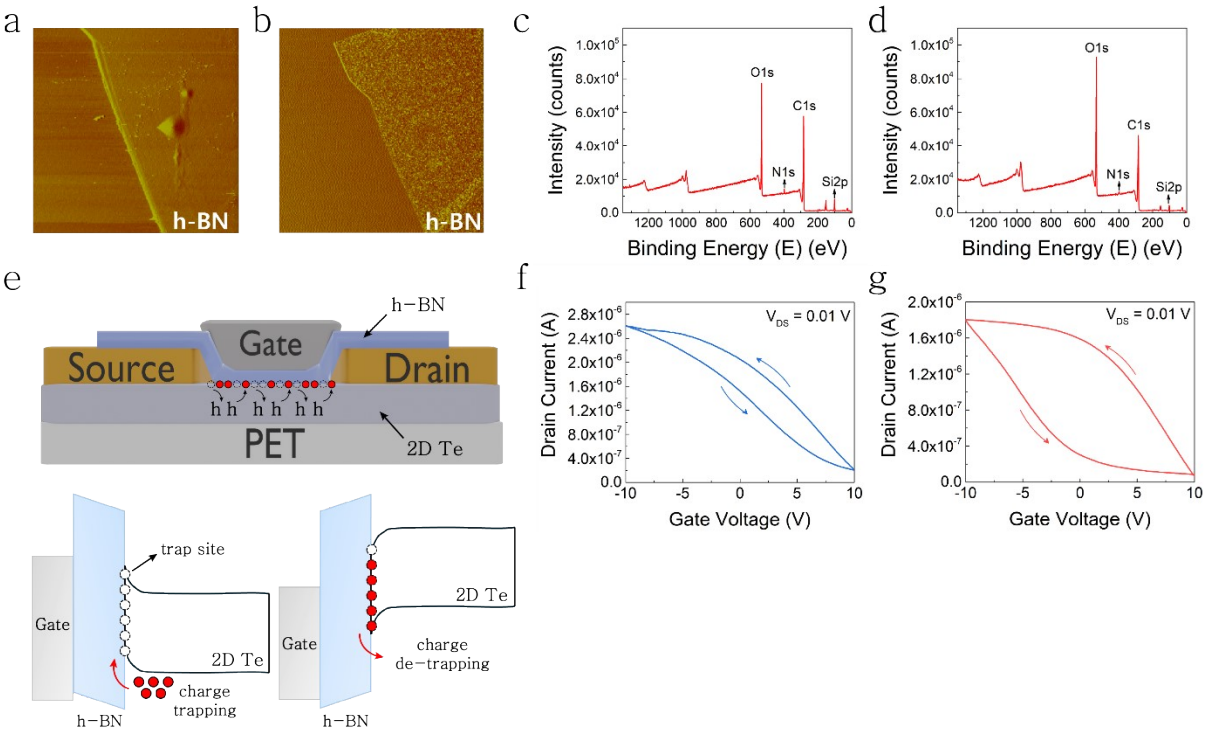

Figure S5. (a, b) AFM friction image and (c, d) XPS showing the comparison before and after O_2 plasma treatment on h-BN. (e) Schematic diagram and energy band structures of the charge-trapping/de-trapping between the 2D Te channel and h-BN interface. Hysteresis characteristics (f) before and (g) after O_2 plasma treatment.

The AFM friction image and XPS data illustrate the surface changes of h-BN induced by O2 plasma treatment. As a result of increased defects on the h-BN surface due to O2 plasma treatment, trap sites at the Te/h-BN interface increase, and this interface acts as a charge trapping layer. Consequently, charge trapping/de-trapping occurs at this charge trapping layer, enabling modulation of channel conductivity.[1] A comparison of hysteresis curves before and after O2 plasma treatment was conducted to support this explanation. In Figure S5 (f), a low defect structure between the h-BN and Te layers resulted in observed hysteresis ratio and window of 1.35 and 3.6, respectively. In contrast, Figure S5 (g) demonstrates a clear increase in hysteresis ratio and window to 5.25 and 10.42, respectively, attributed to the generation of defects on the h-BN surface after O2 plasma treatment.

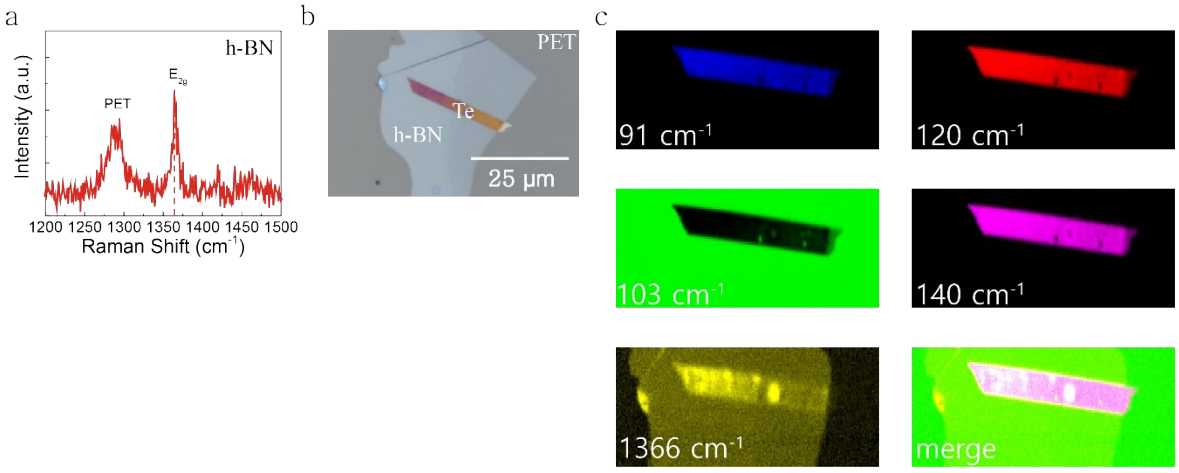

Figure S6. (a) Raman spectra of h-BN on a PET substrate. (b) Optical image and (c) Raman mapping images of 2D Te encapsulated with h-BN on a PET substrate.

The Raman spectra shown in Figure S6 (a) exhibit an intense peak at 1366 cm^{-1}, which corresponds to the E_{2g} vibration mode of h-BN.[2]

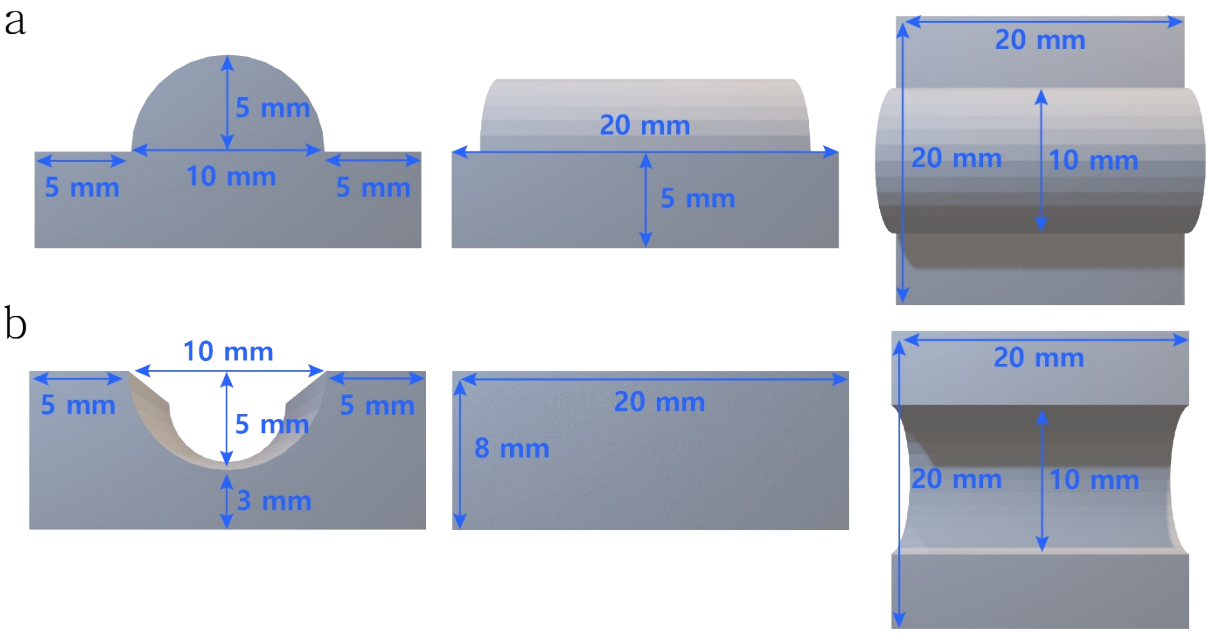

Figure S7. Schematics of (a) convex and (b) concave bending models at a bending radius of 5 mm on the experimental bending fixture.

Calculation of curvature

The bending stability of the flexible 2D Te synaptic transistor was measured using concave and convex models, as shown in Figure S7. The bending strains of the concave and convex models were calculated using the following equation:[3]

$$\varepsilon = \frac{t}{\rho},$$

where ε, t, and ρ represent the range of the strain, substrate thickness, and bending radius, respectively. The thickness of the flexible PET substrate is 100 μm, and the bending radius is 5 mm, which presents a calculated curvature of 2%.

Table S1. Gate tunability performance summary of flexible 2D Te synaptic transistor of linearity, dynamic ranges, asymmetry ratio, and effective states.

	Potentiation nonlinearity	Depression nonlinearity	Dynamic ranges (G_{max}/G_{min})	Asymmetry ratio	Effective conductance states
Figure 5a	4.17	4.13	1.08	0.65	42
Figure 5b	4.22	3.50	1.06	0.59	40
Figure 5c	1.60	3.81	10.5	0.27	85
Figure 5d	0.34	1.90	1.06	0.2	93
Figure 5e	0.05	1.54	1.05	0.2	93

Table S2. Performance comparison of previously reported 2D material-based synaptic device.

Active materials	Structure	Substate	Power	Nonlinearity	Recognition accuracy	Flexibility	Ref
Te	Three-terminal	PET	9 fJ	0.05/1.54	93 %	O	This work
ReS_2	Two-terminal	PDMS	0.56 pJ	0.1/-	~92 %	O	[4]
Pyr-GDY/Gr/PbS-QDs	Two-terminal	PET	-	1.7/1.9	90.8 %	O	[5]
$MoS_2/LiSiO_x$	Three-terminal	CPI	0.55 nJ	0.55/-1.00	95.2%	O	[6]
WSe_2	Three-terminal	Si	532 fJ	1.4/1.4	~90 %	X	[1]
$MoTe_2$	Three-terminal	Si	-	-1.24/2.4	81 %	X	[7]

Table S3. Performance summary of convex and concave bending of 2D tellurium flexible FET includes linearity, dynamic range, asymmetry ratio, and effective state.

	Potentiation nonlinearity	Depression nonlinearity	Dynamic ranges (G_{max}/G_{min})	Asymmetry ratio	Effective conductance states
Convex bending	-0.25	0.72	1.05	0.06	100
Concave bending	-1.83	2.18	1.04	0.1	79

Reference

1. S. Seo, S.-H. Jo, S. Kim, J. Shim, S. Oh, J.-H. Kim, K. Heo, J.-W. Choi, C. Choi and S. Oh, *Nature Communications*, 2018, **9**, 5106.
2. S. Veeralingam, L. Durai, P. Yadav and S. Badhulika, *ACS Applied Electronic Materials*, 2021, **3**, 1162-1169.
3. J. M. Gere and B. J. Goodno, *Mechanics of materials*, Cengage learning, 2012.
4. S. Seo, J. J. Lee, R. G. Lee, T. H. Kim, S. Park, S. Jung, H. K. Lee, M. Andreev, K. B. Lee and K. S. Jung, *Advanced Materials*, 2021, **33**, 2102980.
5. Y.-X. Hou, Y. Li, Z.-C. Zhang, J.-Q. Li, D.-H. Qi, X.-D. Chen, J.-J. Wang, B.-W. Yao, M.-X. Yu and T.-B. Lu, *ACS nano*, 2020, **15**, 1497-1508.
6. Y. Hwang, B. Park, S. Hwang, S. W. Choi, H. S. Kim, A. R. Kim, J. W. Choi, J. Yoon, J. D. Kwon and Y. Kim, *Small Methods*, 2023, **7**, 2201719.
7. J. Gao, X. Lian, Z. Chen, S. Shi, E. Li, Y. Wang, T. Jin, H. Chen, L. Liu and J. Chen, *Advanced Functional Materials*, 2022, **32**, 2110415.